Tipping Water Balance and the Pt Loading Effect in Polymer Electrolyte Fuel Cells: A Model-based Analysis

Tasleem Muzaffar[1], Thomas Kadyk[2], and Michael Eikerling [1*]

[1]*Department of Chemistry, Simon Fraser University, Burnaby, British Columbia, Canada*

[2]*Institute of Energy and Process Systems Engineering, Technische Universität Braunschweig, Braunschweig, Germany*

[*]*meikerl@sfu.ca*

February 19, 2018

Abstract

The commercial deployment of polymer electrolyte fuel cells (PEFCs) hinges on breakthroughs in design and integration of highly performing and durable catalyst layers with drastically reduced platinum loading. Experimental studies have shown an unexpected increase in voltage losses upon a drastic reduction in the Pt content. In an effort to unravel this peculiar behavior, an existing physical model of catalyst layers in PEFCs is employed to analyze a wide range of fuel cell performance data from the literature. The analysis reveals correlated trends in key fuel cell parameters. These findings can be explained in view of the tipping water balance that affects the interplay of transport and reaction in catalyst layer and gas diffusion media. This represents a compelling alternative to the widespread ionomer-film hypothesis that links observed power losses at low Pt loading to a mesoscopic oxygen transport resistance. The presented theoretical analysis warrants the definition of a correlation exponent that should find use in assessing the merit of different approaches in catalyst layer fabrication.

Following the footprints in numerous reports of the Department of Energy[1] and in peer-reviewed articles,[2–4] the highly original and once coveted design of membrane-electrode assemblies (MEAs) developed by the company 3M should have levered a breakthrough in polymer electrolyte fuel cell (PEFC) technology. 3M MEAs with nanostructured thin film electrodes showed impressive gains in performance and durability combined with excellent prospects for production scale-up.[5] What's more, the platinum loading at the cathode catalyst layer (CCL) that performs the notoriously sluggish oxygen reduction reaction (ORR) undercut the loading of conventional layers by about a factor 10.[2] The 3M approach to MEA fabrication has been the most impressive demonstration to date that a drastic reduction of Pt loading, m_{pt}, is achievable without sacrificing performance, as these MEAs indeed exhibited the highest power performance reported to date[2]. However liquid water removal clearly transpired as the Achilles heel of catalyst layer design[6]. Moreover, the 3M design demonstrated an important principle of catalyst layer operation: liquid water is sufficient as the medium for proton transport in the catalyst layer.[7–9]

In the conventional cell layout, the Pt-based catalyst contributes about $40\% - 50\%$ to the cost of a PEFC stack manufactured at high volume.[1] Moreover, the ORR at the cathode incurs about $30\% - 40\%$ of the voltage losses during operation, as can be gleaned from a polarization curve analysis.[10] The pioneering 3M technology triggered an avalanche of activities in catalyst layer research[11–16] with a common mission: bringing down the demand of Pt to a level that renders its cost and limited abundance insignificant, while improving, or at least preserving,

power performance and durability.

At this point, none of these strategies in materials modification and catalyst layer fabrication constitutes a resounding success. Promising results in laboratory tests were not reproduced in tests under typical fuel cell operating conditions or the improvements failed to transpire at the level of fuel cell stack operation – where it matters. A presumed culprit for the unexplained, additional losses was found: a thin ionomer film covering the Pt particles, causing a strong local transport resistance[17–24]. This unverified hypothesis spread and solidified rapidly in the community with large research efforts dedicated to follow-up work.

However, this article exposes an alternative and more general explanation of the m_{pt} effect: a tipping water balance in catalyst layers with ultra-low m_{pt} i.e. ($m_{\mathrm{pt}} < 0.1$ mg cm^{-2}). This hypothesis emerges from the presented modeling-based analysis that assesses the impact of a reduction in m_{pt} on electrochemical performance for a wide range of approaches in CCL design and fabrication. The analysis unravels the concerted impact of the core set of parameters that control catalyst layer operation. The revealed trends in parameter variation are the key to a much-needed mechanistic interpretation of the m_{pt} effect.

Strategies to achieve a Pt loading reduction

A drastic reduction of m_{pt} can be achieved via two principal modification strategies:

(1) reduction of catalyst layer thickness, L_{CCL}, at constant composition, i.e., fixed volume fractions of catalyst, support, ionomer, and pores;[25–36]

(2) dilution of catalyst at constant L_{CCL} , i.e., reduction of the catalyst volume fraction.[31–33]

In practice, a significant m_{pt} reduction is usually achieved by an unknown blend of these

strategies.

Evidently, L_{CCL} should be considered as a key parameter to monitor in this context. Usually, drastic changes in m_{pt} will come along with other structural modifications of the CCL, as is obvious for thin-film substrates like the 3M nanowhisker morphology[2–4] or nanoporous metal structures.[37–39]

Thick and thin electrodes: basic concepts

From a modeling perspective, it is instructive to categorize catalyst layers into two classes: gas diffusion electrodes (GDEs) and flooded porous electrodes (FPEs). GDEs consist of three interpenetrating and percolating phases (solid, electrolyte and gas phase). GDE-type CCLs are impregnated with ionomer and they have typical thickness of $5 - 10\,\mu$m. A GDE-type CCL will operate well only if reactant supply via gas diffusion is guaranteed; it will fail if liquid water blocks percolating pathways of gaseous diffusion.

FPE on the other hand do not contain a separate percolating gas-phase and the reactant gas dissolves in water-filled pores at the interface with the gas diffusion layer (GDL). An FPE-type CCL is usually ionomer-free and has much reduced thickness, $L_{\mathrm{CCL}} \sim 50 - 300$ nm. This small thickness drastically lowers the requirement on oxygen diffusivity, rendering oxygen transport through the liquid water phase sufficient. A CCL of this type will exhibit its best electrochemical performance if it is fully flooded with liquid water, thus utilizing all of the available catalyst surface area. Ionomer impregnation of FPEs is not needed, as the proton demand of the reaction can be satisfied by proton transport in water-filled pores.[7,8,40] The distinction of GDEs and FPEs alludes to the important role of water as the pore filling liquid

and it underlines the importance of the liquid saturation, S_r, as a critical composition variable to determine effective properties of the layer. S_r needed for optimal performance of a catalyst layer is intimately tied to its thickness. Here, we will briefly discuss, in a qualitative fashion, the impact of S_r on catalyst layer performance, following more detailed treatments of water phenomena in PEFC electrodes in Refs.[41–46] A detailed quantitative treatment of the impact of S_r is beyond the scope of this article.

An FPE-type CCL, in which $S_\mathrm{r} = 1$,[46] must be ultrathin for the liquid water phase to warrant a sufficiently high diffusion flux of dissolved oxygen. Moreover, efficient operation of an FPE-based MEA demands an adjacent gas diffusion medium with high vaporization capability. If S_r approaches 1 in a GDE-type CCL, oxygen flux will be drastically impaired.[41,43,44] Therefore, the porous electrode layers will be more prone to flooding with dramatic consequences for oxygen supply and overall ORR activity. The layers analyzed in this article are all of GDE-type.

A vital concept to rationalize the aforementioned interdependence of S_r and L_CCL is the reaction penetration depth due to oxygen diffusion, defined as[42]

$$\lambda_\mathrm{p} = \frac{4\mathrm{F}D_{\mathrm{O_2}}^{\mathrm{CCL}} p_{\mathrm{O_2}}^{\mathrm{o}}}{j_0 \mathrm{R}T}, \tag{1}$$

where F is the Faraday constant, R the ideal gas constant, T the temperature, $D_{\mathrm{O_2}}^{\mathrm{CCL}}$ the effective oxygen diffusion coefficient of the CCL, $p_{\mathrm{O_2}}^{\mathrm{o}}$ the oxygen partial pressure at the interface between CCL and GDL, and j_0 the operating current density. A GDE-type CCL at $T = 350$ K, $j_0 = 1$ A cm^{-2}, $D_{\mathrm{O_2}}^{\mathrm{CCL}} = 2.5 \times 10^{-4}$ cm^2 s^{-1} and $p_{\mathrm{O_2}}^{\mathrm{o}} = 1$ bar has $\lambda_\mathrm{p} \sim 33$ μm, whereas an FPE-type CL under the same conditions but at $D_{\mathrm{O_2}}^{\mathrm{CCL}} = 2.3 \times 10^{-5}$ cm^2 s^{-1}, and

$p^{o}_{O_2} = 3.38 \times 10^{-2}$ bar, exhibits $\lambda_p \sim 100$ nm. The value of $p^{o}_{O_2}$ used for FPE-type CCL accounts for dissolution of O_2 in water with Henry law constant, $H_{O_2} = 1.3 \times 10^{-3}$ L^{-1} bar^{-1} mol. When $\lambda_p \ll L_{CCL}$, the reaction is limited to a portion of the CCL near the GDL interface and the rest of the CCL is not utilized. For $\lambda_p \geq L_{CCL}$, the reaction rate is distributed uniformly throughout the CCL. Optimal Pt utilization will be achieved with $\lambda_p \geq L_{CCL}$.

What is the impact of the type and thickness of the CCL on cell operation?

At given j_0, a thick GDE has a low volumetric current density and a high vaporization capability owed to a highly developed liquid-gas interface in the partially flooded pore space.[43,44] Upon reduction of L_{CCL}, the volumetric current density grows as $j_0 \propto (L_{CCL})^{-1}$. At the same time, the vaporization capability of the layer decreases proportionally to L_{CCL} at first. This results from the decrease of the liquid-vapor interfacial area under constant S_r, as indicated in Figure 1 (a) . Upon further reduction of L_{CCL}, as S_r increases the vaporization capability decreases over-proportionally until it reaches zero under fully flooded conditions.

To clarify the last point, let us consider a ten-fold reduction of L_{CCL}; then the ratio of the rate of water production to the rate of vaporization will increase by at least two orders of magnitude. Inevitably, more liquid water has to leave the catalyst layer aggravating problems with flooding in the GDL as seen in Figure 1 (a). In order to understand the impact of CCL modification and especially of changes in L_{CCL} on PEFC operation, it is crucial to closely monitor changes in water distribution, not only in the CCL, but in the whole cell, especially the GDL and flow channels on the cathode side.

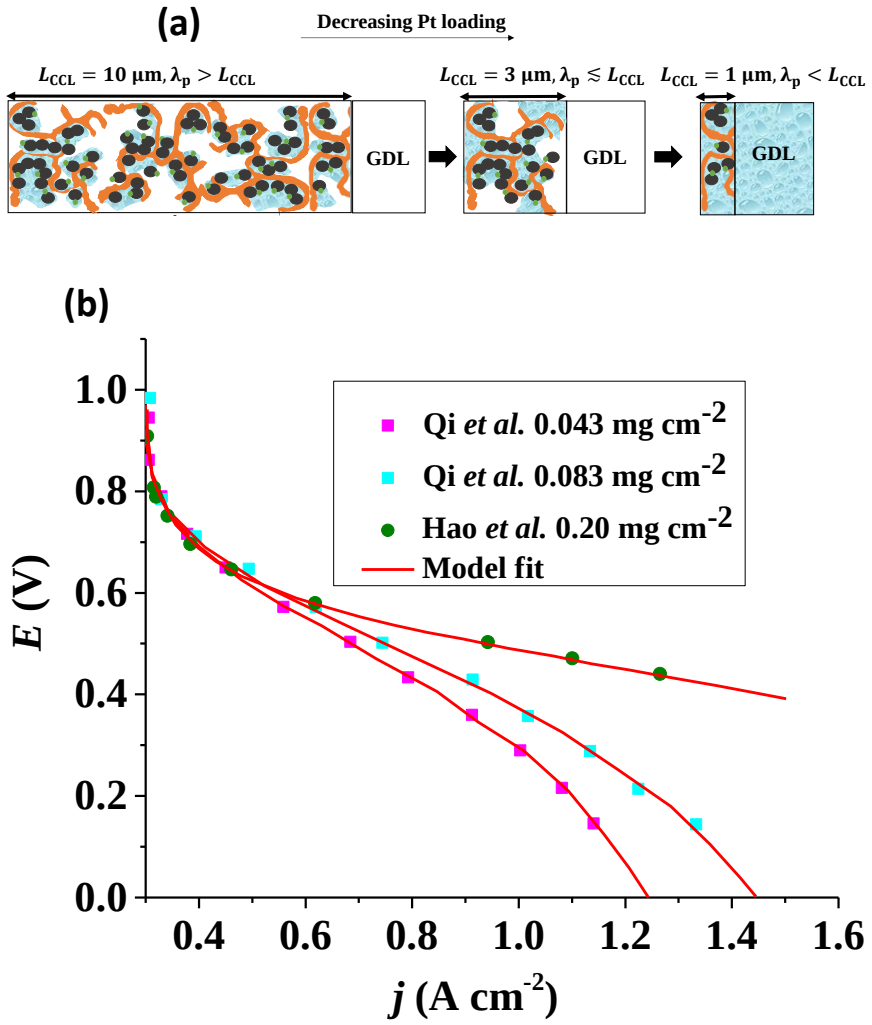

Figure 1: **(a)** Schematic of CCL|GDL configuration in different regimes of CCL thickness and water accumulation. The picture on the left corresponds to ideal operation of a relatively thick CCL ($L_{CCL} = 10\ \mu m$). As the vaporization capability wanes with the L_{CCL} reduction, more liquid water will accumulate first in the CCL **(a-2)** and then in the adjacent diffusion medium **(a-3)**. **(b)** Fits of fuel cell polarization curves extracted from Refs.[25–36] with the physical models developed in Refs.[10,41–45,47–49] and implemented as an executable routine in Ref.[48] Only a subset of experimental studies that were analyzed are shown; fits for all the different sets of experimental data analyzes are provided as Supporting Information. These fits were used to extract the parameters that change in response to the variation in m_{pt} viz. $D_{O_2}^{GDL}$, $D_{O_2}^{CCL}$, j_{eff}^{0}, and σ_{el}.

Modeling capabilities

The genealogy of physical models of CCL operation traces back to the beginnings of porous electrode theory, as reviewed in Ref.[10] Over time, CCL models have been developed and refined specifically to incorporate structure vs. property relations based on percolation theory,[41,42,47] treat water phenomena,[43,44] and account for the self-consistent coupling of transport phenomena and reaction conditions at different scales.[45] A range of analytical solutions of CCL models have been obtained[10,42,47–49] and model-based tools to analyze fuel cell polarization curves have been demonstrated.[48]

If sufficient information on thickness, composition, and pore space morphology is available, CCL models are capable to closely reproduce fuel cell polarization curves, as demonstrated in Refs.[10,45,48] Based on high-quality fits of the physical model to experimental polarization curves, the basic parameters of the CCL including proton conductivity, oxygen diffusivity and exchange current density were determined in those works. Further model-based analysis could then be applied to generate a voltage loss breakdown, calculate the effectiveness factor of Pt utilization, and plot the spatial map of catalyst activity in the layer. However, in spite of analytical capabilities of existing models they have never been employed to perform comprehensive analyses of large experimental data sets. The exploration of the m_{pt} effect for a wide range of experimental studies is an excellent case to demonstrate model capabilities. To this end, we have evaluated various data sets from recent literature sources.[25–36]

We have adopted the physical model developed through various generations in Refs.[10,41–45,47–49] and implemented by Kulikovsky in Ref.[48] to analyze the performance data of PEFCs with

varying m_{pt}. We have considered four parameters as variable and used them for fitting of experimental data. They are the exchange current density, j^0_{eff}, proton conductivity in CCL, σ_{el}, as well as the oxygen diffusion coefficient in CCL, $D^{CCL}_{O_2}$, and GDL, $D^{GDL}_{O_2}$.

Comparison with experiment

All layers that were analyzed are GDE type electrodes. Model fits of experimental polarization curves are shown in Figure 1 (b) for a subset of experimental studies. The complete set of fits and parameters for all experimental studies[25–36] are provided in the supplementary information, SI. Figure 2 depicts the variation of physical properties extracted from the fitting. The following trends can be discerned:

(1) The proton conductivity, σ_{el} remains relatively constant with the reduction in m_{pt}. Since water is the medium for proton conduction, increased water accumulation is not expected to exert a detrimental effect on proton conductivity.

(2) In studies with strong correlation between m_{pt} and L_{CCL}, the oxygen diffusion coefficient in the GDL, $D^{GDL}_{O_2}$, exhibits a marked decrease when m_{pt} is reduced to below 0.1 mg cm^{-2}.[25,26,30,32,33,35] In this scenario, more liquid water flows out of the CCL because of its diminished vaporization capability. As a consequence, more liquid water will accumulate in the GDL resulting in its flooding, hence blocking pathways for the gaseous supply of oxygen. The large scatter in values of $D^{GDL}_{O_2}$ for different studies can be explained by different MEA fabrication methods and different types of GDL used; details for each system can be found in SI. We also applied the model-based analysis to MEAs fabricated by the direct membrane deposition method of Klingele *et al.*[50] and Breitwieser *et al.*[51] In this case, $D^{GDL}_{O_2}$ remains constant with the reduc-

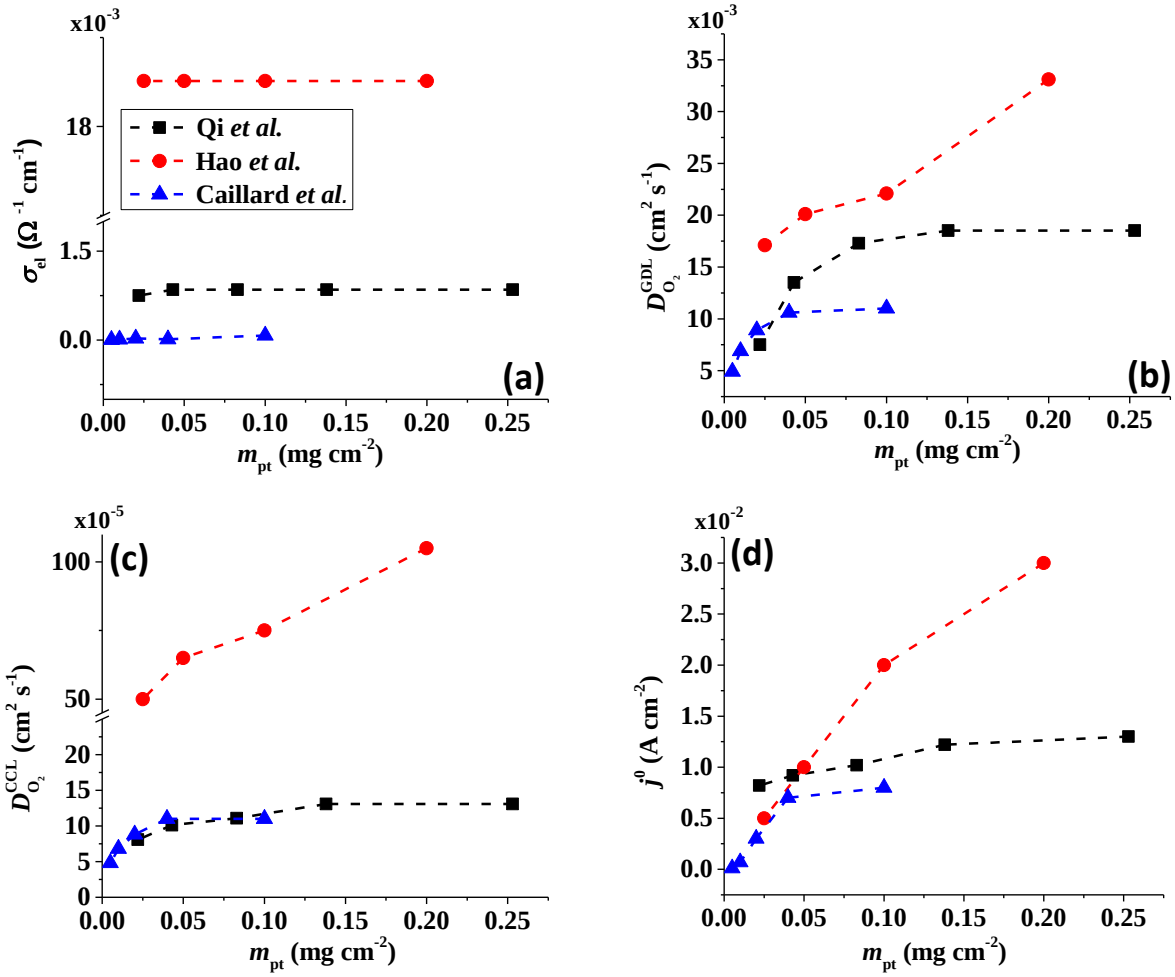

Figure 2: Effect of m_{pt} on **(a)** σ_{el}, **(b)** $D_{O_2}^{GDL}$, **(c)** $D_{O_2}^{CCL}$, **(d)** j_{eff}^{0}.

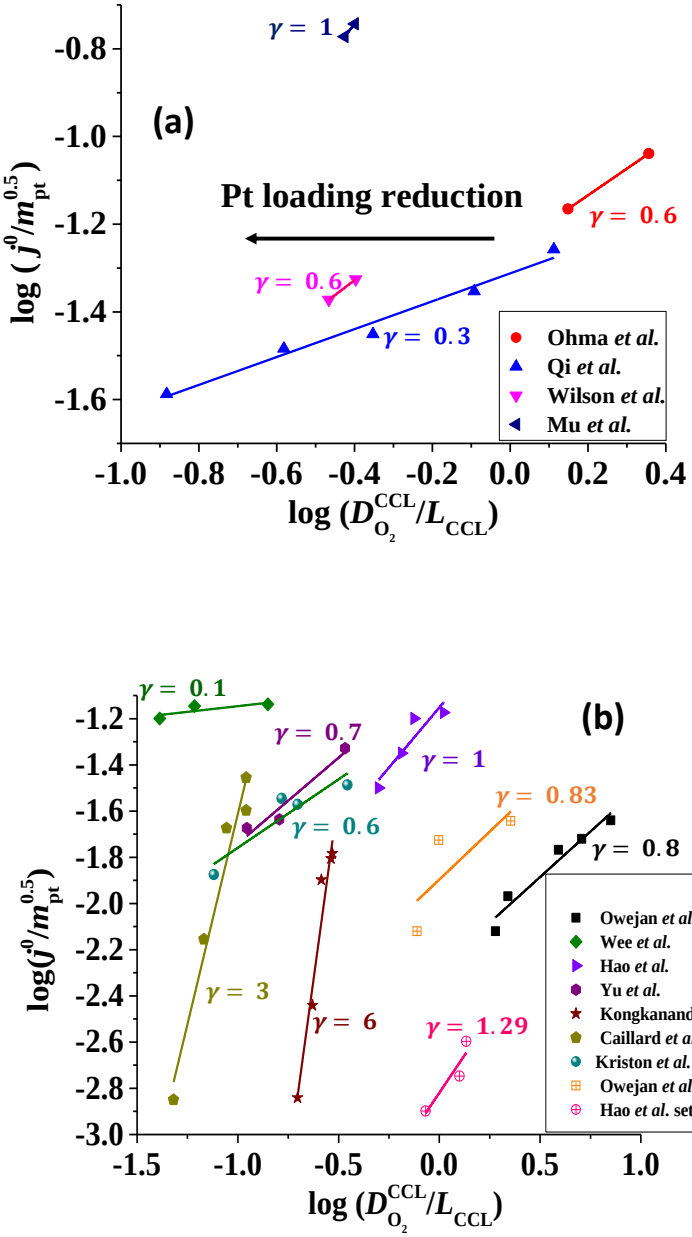

Figure 3: Log-log plot of $\frac{D_{O_2}^{CCL}}{L_{CCL}}$ vs. $\frac{j_{eff}^{0}}{m_{pt}^{0.5}}$ for experimental studies with **(a)** $L_{CCL} \propto m_{pt}$, where $L_{CCL} = 10\ \mu$m was used as a reference at $m_{pt} = 0.2$ mg cm^{-2} and **(b)** fixed $L_{CCL} = 10\ \mu$m.

tion in m_{pt} as can be seen in SI. This can be explained by enhanced water removal from the CCL via transport of water towards the anode side that is enabled by the extremely thin and highly permeable PEM employed in that study.

(3) Similarly, $D_{O_2}^{CCL}$ exhibits a decrease with decreasing m_{pt} in studies with strong correlation between m_{pt} and L_{CCL}. This effect can be explained with the diminished vaporization capability and the correspondingly increased S_r in the CCL that inhibits the gaseous transport of oxygen. Based on equation 1, flooding of the CCL results in $\lambda_p \ll L_{CCL}$. This situation is described well with modeling approaches presented in Refs.[10,42,47] that predict a doubling of the Tafel-slope in this thickness regime.

(4) Interestingly, the trend observed in the effective exchange current density, j_{eff}^0 follows the trend in $D_{O_2}^{CCL}$. It has been long-observed albeit remained unexplained that kinetic voltage losses upon reduction of L_{CCL} increase by an amount that exceeds the extent expected based on the pure geometric effect of the reduction in electrochemically active surface area. Where do the additional "kinetic" losses upon L_{CCL} reduction come from? To resolve this issue, we must consider the interplay of electrochemical kinetics and oxygen diffusion in the CCL.

The generic exchange current density of a CCL is given by[10]

$$j^0 = j_*^0 m_{pt} \delta, \quad \delta = \frac{N_A}{M_{pt} \nu_{pt}} \Gamma_{np} \Gamma_{stat}. \tag{2}$$

where j_*^0 is the intrinsic exchange current density, N_A the Avogadro constant, M_{pt} the atomic mass of Pt, Γ_{np} the surface-to-volume atom ratio of Pt nanoparticles, Γ_{stat} the statistical utilization of Pt particles, and ν_{pt} the number of Pt atoms per units surface area of the catalyst.

Severe starvation of the oxygen flow on its path through the catalyst layer brings about a

doubling of the Tafel-slope in the polarization curve, as explained in Refs.[10,47]. Furthermore, the doubling of the Tafel-slope entails a modification of the effective exchange current density that results in[10]

$$j^0_{\text{eff}} = 2\left(\frac{4 j^0_* m_{\text{pt}} \text{F} p^{\text{o}}_{\text{O}_2} \delta}{\text{R}T}\right)^{0.5} \left(\frac{D^{\text{CCL}}_{\text{O}_2}}{L_{\text{CCL}}}\right)^{0.5}. \tag{3}$$

Moreover, a reduction of m_{pt} increases the propensity of the CCL for flooding. The corresponding decrease of $D^{\text{CCL}}_{\text{O}_2}$, discussed in the previous paragraph, will lead to a situation with $\lambda_{\text{p}} \ll L_{\text{CCL}}$. This effect introduces another factor $\frac{\lambda_{\text{p}}}{L_{\text{CCL}}}$ in the effective exchange current density,

$$j^0_{\text{eff}} = 2\left(\frac{4 j^0_* m_{\text{pt}} \text{F} p^{\text{o}}_{\text{O}_2} \delta}{\text{R}T}\right)^{0.5} \left(\frac{D^{\text{CCL}}_{\text{O}_2}}{L_{\text{CCL}}}\right)^{0.5} \frac{\lambda_{\text{p}}}{L_{\text{CCL}}}. \tag{4}$$

Using λ_{p} as defined in equation 1 and re-arranging results in

$$j^0_{\text{eff}} = 2\frac{(m_{\text{pt}} j^0_* \delta)^{0.5}}{j_0} \left(\frac{4\text{F} p^{\text{o}}_{\text{O}_2}}{\text{R}T}\right)^{1.5} \left(\frac{D^{\text{CCL}}_{\text{O}_2}}{L_{\text{CCL}}}\right)^{1.5}. \tag{5}$$

Equation 5 includes two superimposed effects: the first one is a transmission line effect, which results in a doubling of the Tafel-slope and an effective exchange current density given by equation 3; the second effect accounts for the change of λ_{p}, which is inversely proportional to j_0. Now depending upon the operation regime, the exponent on the two right most terms of the equation 5 is expected to vary between 0 to $\frac{3}{2}$. For convenience, we introduce a correlation exponent, γ with an expected range $0 \leq \gamma \leq \frac{3}{2}$,

$$j_{\mathrm{eff}}^{0} = 2\frac{(m_{\mathrm{pt}} j_{*}^{0} \delta)^{0.5}}{j_0} \left(\frac{4\mathrm{F} p_{\mathrm{O_2}}^{\mathrm{o}}}{\mathrm{R}T}\right)^{\gamma} \left(\frac{D_{\mathrm{O_2}}^{\mathrm{CCL}}}{L_{\mathrm{CCL}}}\right)^{\gamma}. \tag{6}$$

Based on the foregoing analysis, the value of γ allows for three cases to be distinguished:

1. Electrode operation in the purely kinetic regime (excellent oxygen transport, $\lambda_{\mathrm{p}} > 3\, L_{\mathrm{CCL}}$) results in $\gamma \simeq 0$.

2. Electrode operation in the intermediate regime with nonlinear interplay of reaction and diffusion, indicated by double Tafel slope behavior ($\lambda_{\mathrm{p}} \lesssim L_{\mathrm{CCL}}$), the first effect is present, results in $\gamma \simeq \frac{1}{2}$. and

3. Electrode operation in the oxygen starvation regime with $\lambda_{\mathrm{p}} \ll L_{\mathrm{CCL}}$, where both effects will be present and the total effect will be a superposition of both (or mathematically a multiplicative effect), results in $\gamma \simeq \frac{3}{2}$.

By assessing the value of γ, we can see where we are on that scale from 0 to $\frac{3}{2}$ and determine which effects of oxygen depletion and starvation occur in a particular type of electrode. A prerequisite for the use of equation 6 is that the comparison of different electrodes using this relation is done at the same operating current density j_0.

The first case ($\gamma \simeq 0$) represents excellent catalyst utilization, whereas the second case ($\gamma \simeq \frac{1}{2}$) corresponds to a CCL that would exhibit high power performance[47]. The third case ($\gamma \simeq \frac{3}{2}$), obviously, signifies poor catalyst effectiveness as well as poor performance. Good catalyst layer design demands $0 \leqslant \gamma \leqslant \frac{1}{2}$.

The correlation described by equation 6 is tested in Figure 3. The slopes determined from the

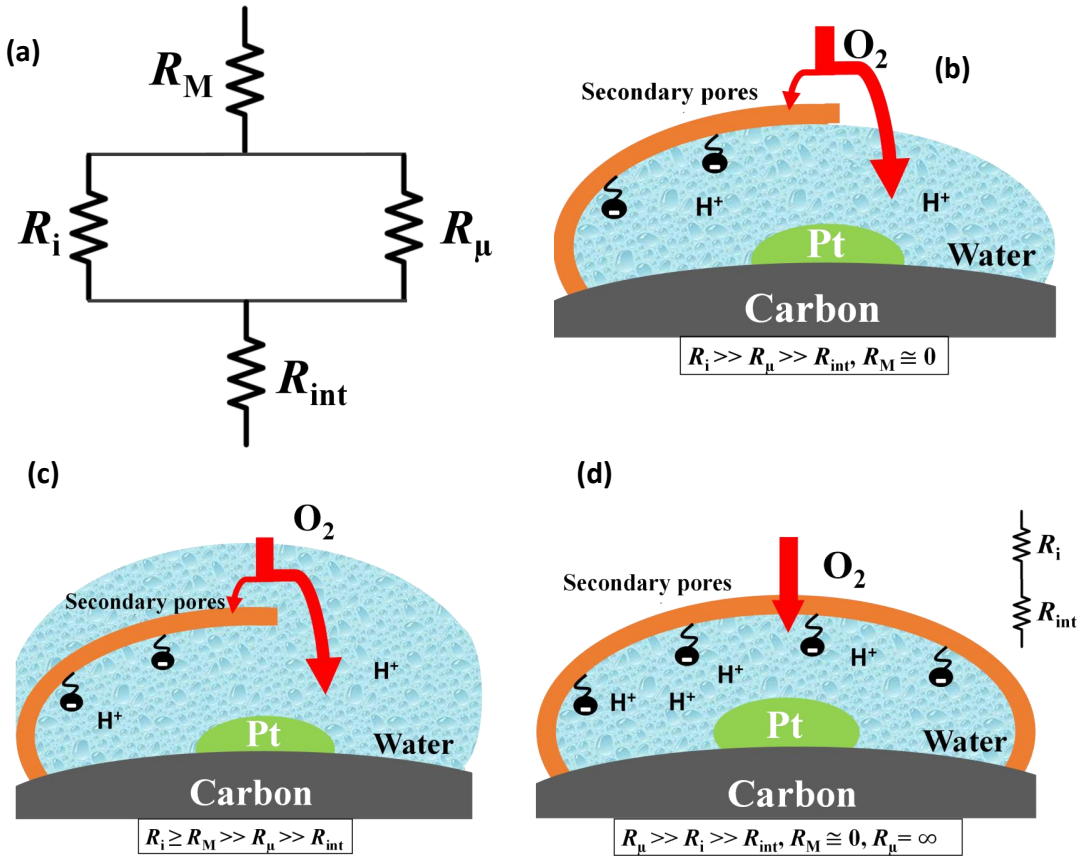

Figure 4: **(a)** Equivalent resistor network representation of oxygen fluxes at the mesoscale. R_i, R_M, R_μ, R_{int} are ionomer resistance, secondary pore resistance, primary pore resistance, and interfacial resistance to oxygen diffusion respectively. Schematic of oxygen transport **(b)** for a situation with partial ionomer coverage and parallel diffusion paths through ionomer film or water-filled primary pore. The latter pathway could constitute a low resistive pathway of oxygen supply. **(c)** In a situation with water-filled secondary pores, the high macroscopic diffusion resistance evoked by the flooding will limit electrode performance. **(d)** In a peculiar situation with complete encapsulation of Pt site by ionomer, the rate of oxygen supply will be limited by the oxygen permeation rate through the ionomer film.

log-log plot of $\frac{j^0_{\mathrm{eff}}}{m^{0.5}_{\mathrm{pt}}}$ vs $\frac{D^{\mathrm{CCL}}_{\mathrm{O_2}}}{L_{\mathrm{CCL}}}$ corresponds to the values of γ shown at the plots. However, in the experimental studies the values of L_{CCL} are not known. Therefore, we proceeded in two steps. In the first step, the correlations were tested for two limiting scenarios, assuming either

1. constant composition, i.e., assuming $m_{\mathrm{pt}} \propto L_{\mathrm{CCL}}$ using $m_{\mathrm{pt}} = 0.2$ mg cm^{-2} and $L_{\mathrm{CCL}} =$ 10 μm as reference, or

2. Pt dilution at constant $L_{\mathrm{CCL}} = 10$ μm.

To evaluate the values of γ for the studies used in this work, knowledge of relevant scenario in terms of thickness reduction and dilution effects is required. However, for most studies, we did not know *a priori* which scenario would be valid. So an approach by exclusion was employed. We tested each data set for both scenarios. One of the two scenarios resulted in a positive-defined as thus meaningful value of γ, whereas the other scenario yielded an unphysical (a negative) value of γ. Only the solution with physically meaningful γ value (positive) is included in Figure 3.

The log-log plot in Figure 3 reveals the concerted impact of ECSA loss and reduction in λ_{p} upon m_{pt} reduction. The phenomenological exponent γ represents a crucial correlation between transport properties and the effective exchange current density. Small γ implies a weak correlation, whereas large γ implies that a reduction in m_{pt} incurs apparent activity losses that are caused by reduced oxygen transport properties under electrode flooding, embodied in λ_{p}. Based on the presented analyses, a benign catalyst layer design would be achieved with $0 \leqslant \gamma \leqslant \frac{1}{2}$, as this would imply that the m_{pt} reduction could be achieved without prompting drastic changes to the transport properties of the layer. The correlation exponent, γ can thus be

used to assess the design of catalyst layers with ultra-low Pt loading. Systematic experimental studies in which the impact of the m_{pt} change on L_{CCL} and composition is precisely controlled and monitored, and model based analyses, as presented above, would be highly insightful in this regard.

For most of the experimental studies in Figure 3, γ lies in the predicted range from $0.5 - 1.5$. The study by Wee *et al.*[29] exhibits a lower value of γ. The studies of Kongkanand *et al.*[34] and Caillard *et al.*[35,36] show significantly larger values of γ that lie out of the expected range. This observation could be indicative of drastic structural changes associated with the m_{pt} reduction, e.g., catalyst compaction due to particle aggregation, which may impact the value of j_*^0 in equation 2, or encapsulation of Pt particles by carbon or by a dense layer of ionomer. More detailed structural data would be needed to further scrutinize this aspect.

The present modeling exercise yields a well-founded hypothesis: the reduction in m_{pt} strongly affects the water fluxes and distribution in GDE-type CCL and adjacent media. The shifted water balance, which is expected as a logical consequence of the shifting ratio of the volumetric rate of water production to the rate of vaporization, affects effective properties and local reaction conditions in a way that leads to trends seen in Figure 3. Especially, the GDL water balance will be strongly affected by flooding for low m_{pt} systems.

Figure 4 presents a graphical illustration of this hypothesis, comparing various states of flooding at the mesoscale. Figure 4 (a) depicts a resistor network analogue for the oxygen fluxes towards the catalyst. In order to reach the Pt surface, oxygen molecules have to pass a resistance in the macropore space, R_M. Then, in order to enter the micropore space surrounding the catalyst particle, oxygen molecules have to pass the resistance of the ionomer film, R_i, or

bypass this film through the water-filled primary pore space via R_μ. Finally, oxygen molecules diffuse through a resistance posed by the interfacial water layer surrounding the Pt nanoparticle, R_{int}. Even though slightly different network configurations might be drawn, the essential point to maintain is the parallel configuration of R_{i} and R_μ in cases with $R_{\text{i}} \gg R_\mu$, which allows oxygen molecules to bypass the ionomer film. Figure 4 (b) represents the expected typical configuration encountered in a well-functioning GDE with gas diffusion in secondary pores. Figure 4 (c) illustrates the change that occurs upon flooding of a GDE as a consequence of a m_{pt} reduction.

Finally, Figure 4 (d) represents an unlikely special case of scenarios in Figure 4 (b) and (c). It misrepresents the significance of the ionomer-film resistance R_{i}. The idea behind Figure 4 (d) is that a strong local transport resistance could be caused by oxygen diffusion through a thin ionomer film, R_{i} that encapsulates Pt completely. In comparison to Figure 4 (b) and (c) it represents the most restrictive and unlikely scenario of local transport resistances encountered by oxygen molecules on their path towards the Pt surface. This idea surfaced in Ref[17]. Thereafter it triggered an avalanche of follow-up work and adoption.[18–24] Groups from Toyota, and GM have reported similar speculative ideas.[19–21,23,24,34] Ultimately, the ionomer-film hypothesis underlying this case is based on two critical assumptions: 1) the ionomer film poses a severe resistance to oxygen diffusion, meaning that $R_{\text{i}} \gg R_{\text{M}}, R_{\text{int}}$; 2) the ionomer film completely encapsulates the catalyst, thereby blocking any alternative diffusion pathway for oxygen, implying $R_\mu \to \infty$. As for the first assumption, the thickness of the ionomer film is still under debate[22]; however, for realistic film thicknesses, it is highly unlikely it could generate a sufficiently inhibiting effect on oxygen diffusion.[19–21,23,24,34] The second assumption corresponds

to an idealized structure of the ionomer film that is neither observed in experiment nor in MD studies of Malek *et al.*[52,53]. In fact, these MD simulations and other works[54–56] suggest that the skin-type ionomer film only partially covers the microporous agglomerates of Pt/C leaving a pathway for O_2 with finite R_μ. We thus believe that the ionomer-film hypothesis is misconstrued and unnecessarily reduces the more general scenario represented by Figure 4 (b) and (c).

As discussed in Ref.[10], to render the catalyst active, it must be surrounded by liquid water, which functions as a proton shuttle. The liquid phase must be continuously connected to guarantee a sufficient rate of proton supply. The water phase that sustains the continuous proton flux functions equally well as a medium for the transport of oxygen via diffusion as demonstrated by 3M in their thin-film CCL design. Oxygen concentration in water will remain sufficiently high if the length of the diffusion path is $\lesssim 200$ nm. Asphyxiation will occur in CCL with thickness above this range and pores flooded. Any alternative explanation for the poor performance of CCL with low m_{pt} must refute or disprove at least one of the basic statements in this paragraph.

The model-based analysis of polarization data thus prompts a logical alternate explanation to the widespread ionomer resistance hypothesis. It is not exclusive and certainly other hypotheses must be scrutinized as well. It should be left to the reader to decide if the hypothesis presented in this work is worth pursuing or other approached should be tried.

Follow up work to understand the mechanistic principles that, underlie our observations and interpretation demand a model that connects the reduction in m_{pt} with associated changes in composition structure, water fluxes, effective properties, and local reaction conditions[43,44].

The work on a such a model is underway in our group.

Summary

This article proposes a conducive strategy for the analysis and interpretation of performance data of CCL with low Pt loading. Physical models were employed to analyze and explain the drastic decline in performance of cathode catalyst layers with small amounts of Pt loaded into them. The study has revealed vital trends and correlations in crucial parameters. Oxygen diffusion coefficients in cathode catalyst layer and gas diffusion layer as well as the exchange current density exhibit a strong decrease with the reduction in Pt loading. These trends can be explained with the loss of vaporization capability in the cathode catalyst layer that leads to a higher liquid saturation in the active layer and more liquid water entering the diffusion medium. Both cathode catalyst layer and gas diffusion layer will thus be flooded which explains the increase in voltage losses due to inhibited oxygen diffusion and diminished effective activity. These results demand a paradigm shift in explaining the voltage losses in ultra-low Pt loading electrodes. The presented alternative hypothesis should initiate a large-scale discussion in the fuel cell community and shape future research directions in the field.

Ideally, for a pursued approach in CCL design and fabrication, a series of CCL with systematically mass-reduced loading of Pt should be made and characterized. Polarization curves obtained should be treated with state-of-the-art performance models to determine the physical parameters of CCL and GDL. The correlation between $\log\left(\frac{j^0_{\text{eff}}}{m^{0.5}_{\text{pt}}}\right)$ and $\log\left(\frac{D^{\text{CCL}}_{\text{O}_2}}{L_{\text{CCL}}}\right)$, should then be analyzed to extract the value of the correlation exponent γ. As a general rule, a small γ implies a CCL structure, in which the Pt loading reduction, is achieved without causing

305 massive transport losses. With this logical strategy outlined, the article should guide the com-
306 munity towards a new generation of systematically planned and analyzed experiments.

Acknowledgments

The authors gratefully acknowledge financial assistance by an Automotive Partnership Canada grant, file number APCPJ417858, that supports the Catalysis Research for Polymer Electrolyte Fuel Cells(CaRPE-FC) network.

Simon Fraser University assisted in meeting the publication costs of this article.

Author Contributions

T.M. and M.E. conceived the research. T.M. applied the model to the experimental data and extracted the physical properties. T.M., T.K., and M.E. analyzed and interpreted results, and wrote and reviewed the manuscript. M.E. supervised the whole project.

Notes

The authors declare no competing financial interest.

Nomenclature

Table 1: Nomenclature

Symbol	Description	Symbol	Description
R	Gas constant	T	Temperature
$D_{O_2}^{CCL}$	Oxygen diffusion coefficient in the CCL	$p_{O_2}^{o}$	Partial pressure of oxygen
F	Faraday Constant	λ_p	Reaction penetration depth
S_r	Liquid water saturation	m_{pt}	Platinum loading
L_{CCL}	Catalyst layer thickness	σ_{el}	Protonic conductivity of electrolyte
$D_{O_2}^{GDL}$	Oxygen diffusion coefficient in the GDL	j_{eff}^{0}	Effective exchange current density
j_*^0	Intrinsic exchange current density	N_A	Avogadro constant
γ	Correlation exponent	Γ_{np}	Surface to volume ratio of nano particles
Γ_{stat}	Statistical utilization of Pt	M_{pt}	Atomic mass of Pt
ν_{pt}	Number of Pt atoms per units surface area	j_0	Current density

References

[1] DOE, *Annual Merit Review Fuel Cell Program*, Department of energy usa, hydrogen and fuel cell programs technical report, 2016.

[2] M. Debe, *Nature*, 2012, **486**, 43–51.

[3] M. Debe, R. Atanasoski and A. Steinbach, *ECS Trans.*, 2011, **41**, 937–954.

[4] M. Debe, *J. Electrochem. Soc.*, 2013, **160**, 522–534.

[5] M. Debe, A. Schmoeckel, G. Vernstrom and R. Atanasoski, *J. Power Sources*, 2006, **161**, 1002–1011.

[6] M. Debe and A. Steinbach, *ECS Trans.*, 2007, **11**, 659–673.

[7] J. Huang, A. Malek, J. Zhang and M. Eikerling, *J. Phys. Chem. C*, 2016, **120**, 13587—-13595.

[8] K. Chan and M. Eikerling, *J. Electrochem. Soc.*, 2011, **1**, B18 – B28.

[9] T. Muzaffar, T. Kadyk and M. Eikerling, *Electrochim. Acta*, 2017, **245**, 1048–1058.

[10] M. Eikerling and A. Kulikovsky, *Polymer Electrolyte Fuel Cells: Physical Principles of Materials Operation*, CRC Press Taylor & Francis Group, 2014.

[11] A. Orfanidi, P. Madkikar, H. El-Sayed, G. Harzer, T. Kratky and H. Gasteiger, *J. Electrochem. Soc.*, 2017, **164**, F418–F426.

[12] H. Su, T. Jao, O. Barron, B. Pollet and S. Pasupathi, *J. Power Sources*, 2014, **267**, 155–159.

[13] S. Shukla, K. Domican, K. Karan, S. Bhattacharjee and M. Secanell, *Electrochim. Acta*, 2015, **156**, 289–300.

[14] T. Huang, H. Shen, T. Jao, F. Weng and A. Su, *Int. J. Hydrogen Energy*, 2012, **37**, 13872–13879.

[15] S. Jiang, B. Yi, L. Cao, W. Song, Q. Zhao, H. Yu and Z. Shao, *J. Power Sources*, 2016, **329**, 347–354.

[16] T. Shu, D. Dang, D. Xu, R. Chen, S. J. Liao, C. Hsieh, A. Su, H. Song and L. Du, *Electrochim. Acta*, 2015, **177**, 168–173.

[17] K. Sakai, K. Sato, T. Mashio, A. Ohma, K. Tamaguchi and K. Shinohara, *ECS Trans.*, 2009, **25**, 1193–1201.

[18] Y. Ono, A. Ohma, K. Shinohara and K. Fushinobu, *J. Electrochem. Soc.*, 2013, **160**, F779–F787.

[19] K. Kudo and Y. Morimoto, *ECS Trans.*, 2012, **50**, 1487–1494.

[20] K. Kudo, R. Jinnouchi and Y. Morimoto, *Electrochim. Acta*, 2016, **209**, 682–690.

[21] R. Jinnouchi, K. Kudo, N. Kitano and Y. Morimoto, *Electrochim. Acta*, 2016, **188**, 767–776.

[22] H. Liu, W. Epting and S. Lister, *Langmuir*, 2015, **31**, 9853–9858.

[23] A. Kongkanand and M. Mathias, *J. Phys. Chem. Lett.*, 2016, **7**, 1127–1137.

[24] A. Weber and A. Kusoglu, *J. Mater. Chem. A*, 2014, **2**, 17207–17211.

[25] A. Ohma, T. Mashio, K. Sato, H. Iden, Y. Ono, K. Sakai, K. Akizuki, S. Takaichi and K. Shinohara, *Electrochim. Acta*, 2011, **56**, 10832–10841.

[26] M. Wilson, *J. Electrochem. Soc.*, 1992, **139**, L28–L30.

[27] Z. Qi and A. Kaufman, *J. Power Sources*, 2003, **113**, 37–43.

[28] S. Mu and M. Tian, *Electrochim. Acta*, 2012, **60**, 437–442.

[29] J.-H. Wee, K.-Y. Lee and S. Kim, *J. Power Sources*, 2007, **165**, 667–677.

[30] H. Yu, J. Roller, W. Mustain and R. Maric, *J. Power Sources*, 2015, **283**, 84–94.

[31] L. Hao, K. Moriyama, W. Gu and C.-Y. Wang, *J. Electrochem. Soc.*, 2015, **162**, F854–F867.

[32] A. Kriston, T. Xie and B. Popov, *Electrochim. Acta*, 2014, **121**, 116–127.

[33] J. Owejan, J. Owejan and W. Gu, *J. Electrochem. Soc.*, 2013, **160**, F824–F833.

[34] A. Kongkanand, N. Subramanian, Y. Yu, Z. Liu, H. Igarashi and D. Muller, *ACS Catal.*, 2016, **6**, 1578–1583.

[35] A. Caillard, C. Charles, R. Boswell and P. Brault, *J. Phys. D. Appl. Phys.*, 2008, **41**, 185307–185316.

[36] A. Caillard, C. Charles, D. Ramdutt, R. Boswell and P. Brault, *J. Phys. D. Appl. Phys.*, 2009, **42**, 045207–045215.

[37] J. Erlebacher and J. Snyder, *ECS Trans.*, 2009, **25**, 603–612.

[38] J. Erlebacher, M. Aziz, A. Karma, N. Dimitrov and S. Karl, *Lett. to Nat.*, 2001, **410**, 5–8.

[39] A. Garsuch, D. Stevens, R. Sanderson, S. Wang, R. Atanasoski, S. Hendricks, M. Debe and J. Dahn, *J. Electrochem. Soc.*, 2010, **157**, B187–B194.

[40] J. Huang, J. Zhang and M. Eikerling, *Faraday Discuss.*, 2016, **193**, 427–446.

[41] M. Eikerling, A. Iosselevich and A. Kornyshev, *Fuel Cells*, 2004, **4**, 131–140.

[42] M. Eikerling, A. Kornyshev and A. Kulikovsky, *Encyclopeida of Electrochemistry, Ch. 8.2*, VCH-Wiley, 2007, pp. 447–453.

[43] M. Eikerling, *J. Electrochem. Soc.*, 2006, **153**, E58–E70.

[44] J. Liu and M. Eikerling, *Electrochim. Acta*, 2008, **53**, 4435–4446.

[45] E. Sadeghi, A. Putz and M. Eikerling, *J. Electrochem. Soc.*, 2013, **160**, F1159–F1169.

[46] K. Chan and M. Eikerling, *Phys.Chem.Chem.Phys.*, 2014, **16**, 2106–2117.

[47] M. Eikerling and A. Kornyshev, *J. Electroanal. Chem.*, 1998, **453**, 89–106.

[48] A. Kulikovsky, *J. Electrochem. Soc.*, 2013, **161**, F263–F270.

[49] A. Kulikovsky, *J. Electrochem. Soc.*, 2014, **161**, E3171–E3179.

[50] M. Klingele, M. Breitwieser, R. Zengerle and S. Thiele, *J. Mater. Chem. A*, 2015, **3**, 11239–11245.

[51] M. Breitwieser, M. Klingele, S. Vierrath, C. Klose, R. Zengerle and S. Thiele, *IMTEK Present. CaRPE*, 2014.

[52] K. Malek, M. Eikerling, Q. Wang, T. Navessin and Z. Liu, *J. Phys. Chem. C*, 2007, **111**, 13627–13634.

[53] K. Malek, T. Mashio and M. Eikerling, *Electrocatalysis*, 2011, **2**, 141–157.

[54] S. Holdcroft, *J. Chem. Mater.*, 2014, **26**, 381–393.

[55] T. Soboleva, K. Malek, Z. Xie, T. Navessin and S. Holdcroft, *Appl. Mater. Interfaces*, 2011, **3**, 1827 – 1837.

[56] M. Uchida, Y. Fukuoka, Y. Sugawara, N. Eda and A. Ohta, *J. Electrochem. Soc.*, 1996, **143**, 2245–2252.